

Real -Time 3D Echocardiography Processing

MIHAELA LASCU, DAN LASCU

Department of Measurements and Optical Electronics

Department of Applied Electronics

Faculty of Electronics and Telecommunications

Bd. Vasile Pârvan no.2

ROMANIA

mihaela.lascu@etc.utt.ro, dan.lascu@etc.utt.ro

<http://www.etc.utt.ro>

Abstract: - Real-time 3-D echocardiography (RT3DE) opens up the possibility of interactive, fast 3-D analysis of cardiac anatomy and function. However, estimation of 3-D parameters using only 2-D images is based on geometric assumptions about the shape of the heart and is dependent on the exact position of the scanning plane. This produces significant errors and interobserver variability. First attempts to acquire 3-D echocardiographic datasets used freehand scanning. However, freehand echocardiography requires several acquisitions and the addition of 3-D localizing hardware, and can be affected by patient breathing, patient movement, and irregular cardiac cycles. As an alternative to freehand echocardiography, systems that automatically move the ultrasound transducer in a controlled way have been developed alternatives that include fan-like scanning and stepwise rotational scanning. However, at the present time its quantitative power cannot be fully exploited due to the limited quality of the images. In this paper are implemented LabVIEW (Laboratory Virtual Instrumentation Engineering Workbench) algorithms that improve the quality of the image. For the beginning we realise histogram, create line profile, calculate measurement statistics associated with a region of interest in the image, realise 3D real-time view and modify the brightness, contrast and gamma of the acquired image. Finally we implement in LabVIEW edge detection and smoothing averaging.

Key-Words: - Echocardiography, image acquisition, image processing, graphical programming, 3D real-time view, LabVIEW, Vision.

1. Introduction

Echocardiography is a unique noninvasive method for imaging the living heart. It is based on detection of echoes produced by a beam of ultrasound (very high frequency sound) pulses transmitted into the heart. From its introduction in 1954 to the mid 1970's, most echocardiographic studies employed a technique called M-mode, in which the ultrasound beam is aimed manually at selected cardiac structures to give a graphic recording of their positions and movements. M-mode recordings permit measurement of cardiac dimensions and detailed analysis of complex motion patterns depending on transducer angulation. They also facilitate analysis of time relationships with other physiological variables such as ECG, heart sounds, and pulse tracings, which can be recorded simultaneously. A more recent development uses electromechanical or electronic techniques to scan the ultrasound beam rapidly across the heart to produce two-dimensional tomographic images of selected cardiac sections. This gives more information than M-mode about the shape of the

heart and also shows the spatial relationships of its structures during the cardiac cycle. A comprehensive echocardiographic examination, utilizing both M-mode and two dimensional recordings, therefore provides a great deal of information about cardiac anatomy and physiology, the clinical value of which has established echocardiography as a major diagnostic tool.

Echocardiography, also called an echo test, is a test that takes *moving pictures* of the heart with sound waves. Real-time 3-D echocardiography (RT3DE) has recently become available. The first of these systems incorporated a matrix transducer of 512 elements to scan a pyramidal volume. More recently, Philips Medical Systems [1] has introduced a system with a 3000 element-transducer, which currently constitutes the state of the art in RT3DE medical equipment. There is evidence that RT3DE is superior to 2-D echocardiography for the quantification of left and right ventricular volumes and function, and for left and right atrium volumes and function, but in spite of these advantages RT3DE has not yet been adopted as a routine technique in the clinical

practice due to difficult image acquisition, limited image quality and laborious manual data analysis

Today real-time visual processing is becoming possible. This means that vision based behaviour can become more dynamic, opening fertile areas for applications. The camera's medical image is captured by a frame grabber. A frame grabber is a digitizing device within a smart camera or as a separate computer card that converts the output of the camera to digital format, typically a two dimensional array of numbers, corresponding to the luminous level of the corresponding point in the field of view, called pixel, and places the image in computer memory so that it may be processed by the machine vision software.

The software will typically take several steps to process an image. Often the image is first manipulated to reduce noise or to convert many shades of grey to a simple combination of black and white (binarization). Following the initial simplification, the software will count, measure, and/or identify objects, dimensions, anomalies or other features in the image. The software support for the paper was realized in LabVIEW and its specific tools. LabVIEW (abbreviation for Laboratory Virtual Instrumentation Engineering Workbench) a very friendly interfaced program, is a platform and development environment for a visual programming language from National Instruments. The graphical language is named *G*. Originally released for the Apple Macintosh in 1986; LabVIEW is commonly used for data acquisition, instrument control and industrial automation on a variety of platforms including Microsoft Windows, various flavours of Unix, Linux and Mac OS. Echocardiography (ultrasound imaging of the heart) has been one of the driving application areas of medical ultrasound and the literature [14], [15], [16] on methods for automatically segmenting and tracking the left ventricle (the normal chamber assessed for heart disease) is extensive. Most attention has been given to tracking the motion of the endocardium (blood pool/tissue border) to allow for estimation of left ventricular areas/volumes and derived measures such as the ejection fraction and also measures for regional wall motion assessment. In particular, these measures are used in diagnosis and assessment of ischemic heart disease.

Most analysis is based on 2-D acquisitions in which it is implicitly assumed that the principal component of motion is in the plane of the acquisition slice. The standard 2-D diagnostic views used for this are called the parasternal short-axis (SAX), and apical four-chamber (4C), two-chamber (2C), and three-chamber (3C) views. The latter three

are also sometimes referred to as (apical) long-axis (LAX) views.

The quality of data, and hence challenges for segmentation, vary depending on the view due to the anisotropy of ultrasound image acquisition, artefacts such as shadowing from the lungs, and attenuation which can be strong. Segmentation methods should also have strategies for avoiding the papillary muscles. Reliably finding the outer wall (often called epicardial border detection) is much more challenging, particularly from apical views. There are many papers [3], [4], [5], on left ventricle tracking which deal with the tracking/deformation model independent of feature extraction or the imaging modality.

Nowadays, 3D echocardiography is a well-known technique in medical diagnosis. Inexpensive echocardiographic acquisition devices are applied to scan 2D slices rotated along a prescribed direction. Then the discrete 3D image information is given on a cylindrical grid.

Usually, this original discrete image intensity function is interpolated to a uniform rectangular grid and then numerical schemes for 3D image processing operations (e.g. nonlinear smoothing) in the uniform rectangular geometry are used. However, due to the generally large amount of noise present in echocardiographic images, the interpolation step can yield undesirable results [20], [21], [22], [23].

2. Three dimensional echocardiography processing

Due to the presence of the ribs and lungs, which block transmission of ultrasound beams, echocardiographic acquisition can only be performed from certain probe locations or windows. Images acquired from different windows show significantly different structure definition at different locations.

The availability of 3-D echocardiographic data allows the combination of datasets acquired from different windows. In previous work [1], [2], [3] we have shown how this combination of acquisitions increases the amount of information and improves the accuracy of quantitative measurements.

As it is common to registration methods based on voxel similarity measures, our algorithm tries to calculate the geometrical transform that maximizes (minimizes) a voxel similarity (voxel dissimilarity) function $S(T)$. The novel part of the algorithm is the definition of the function to be maximized [2] that is implemented in our paper in LabVIEW and Vision.

To increase capture range and reduce the number of local minima, local phase and orientation differences are combined in a single similarity function. This function takes into account the confidence in orientation estimation, which is dependent on the local phase value. Differences in orientation and phase are accumulated over the whole cardiac cycle, as shown in (1).

$$S(T) = \sum_t A + \mu B \quad (1)$$

where

$$A = \frac{\sum_r W(r,t) [1 - o(I_t(r,t),s) \cdot o(I_f(T(r,t),s))]}{\sum_n W(r,t)},$$

$$B = \frac{\sum_r [1 - \cos(\varphi(I_t(r,t),s) - \varphi(I_f(T(r,t),s)))]}{N_r},$$

$$W(r,t) = \min(\sin^2(\varphi(I_t(r,t),s)), \sin^2(\varphi(I_f(T(r,t),s))))$$

$$o(I(r),s) = \frac{(g_s(r) \cdot h_1(r) \cdot I(r), g_s(r) \cdot h_2(r) \cdot I(r), g_s(r) \cdot h_3(r) \cdot I(r))}{\sqrt{\sum_{i=1}^3 (g_s(r) \cdot h_i(r) \cdot I(r))^2}}$$

$$\varphi(I(r),s) = \arctan 2 \left(\sqrt{\sum_{i=1}^3 (g_s(r) \cdot h_i(r) \cdot I(r))^2}, g_s(r) \cdot I(r) \right)$$

The symbols used above are explained in the following:

μ - controls the relative weight given to the phase and orientation terms;

$W(r,t)$ - contains the relative weights calculated from the orientation confidence;

I_t - target image;

I_f - floating image;

φ - phase angle;

o - normalized orientation vector;

N_r - number of voxels in the 3-D dataset;

$I(r)$ - the intensity of a voxel at spatial location r in the image;

$o(I(r),s)$ - normalized orientation vector calculated at scale s ;

$g_s(r)$ - represents the bandpass filter with a central wavelength s ;

$h_1(r) \dots h_3(r)$ - spatial versions of filters described in [2].

The potential increase in structure definition and completeness can be appreciated in the example of

Fig. 1. In Fig. 1(d) and (e), arrows have been placed to highlight image regions where one of the views shows good definition of the left ventricular wall, while in the other view the structure is barely identifiable. In these regions, a clear advantage will result from the combination of information from both datasets. To achieve the improvements related to multiview combination, it is necessary to perform an accurate registration of the datasets. In Fig. 1, the large differences in appearance between the two images can be appreciated. These differences make the registration process extremely difficult if intensity-based approaches are used.

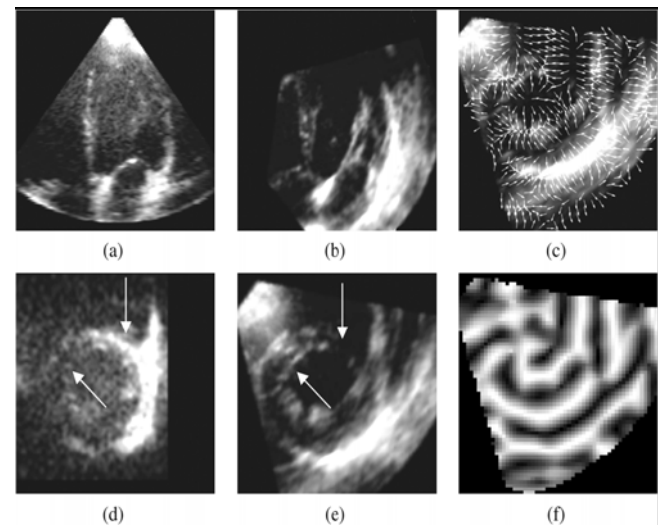


Fig.1. Comparison between different status of the heart.

Comparison of apical [(a) and (d)] and parasternal [(b) and (e)] datasets after registration. (a) and (b) correspond to long axis slices, while (d) and (e) are short axis. Arrows in (d) and (e) show areas that are well defined in only one of the two acquisitions, and would thus benefit from image combination. In (c) and (f), the orientation and phase of the short axis parasternal slice in (e) are shown. Negative/positive phase values correspond to dark/bright pixels, respectively. A mask corresponding to the ultrasound acquisition volume was used to avoid border effects. The implemented 3D view function analyzes the image and displays information for you to review. This function does not modify the image. Displays the light intensity in a three-dimensional coordinate system, where the spatial coordinates of an image form two dimensions and the light intensity forms the third dimension. Each pixel from the image source is represented as a column of pixels in the 3D view. The pixel value corresponds to the altitude.

1. **Northwest**—Sets the viewing orientation for the 3D view in the Northwest direction.
2. **Northeast**—Sets the viewing orientation for the 3D view in the Northeast direction.
3. **Southwest**—Sets the viewing orientation for the 3D view in the Southwest direction.
4. **Southeast**—Sets the viewing orientation for the 3D view in the Southeast direction.
5. **Height**—Maximum height of a pixel drawn in 3D from the image source.

α — Angle between the horizontal axis and baseline. α must be between 0° and 45° .

β — Angle between the horizontal axis and second baseline. β must be between 0° and 45° .
Other kind of processing are:

1. **Reduction** — Sets the size reduction. Reduction is a divisor that is applied to the image source when determining the final height and width of the 3D view image.
2. **Invert** — Inverts the 3D view when selected.

In Fig.2. is represented the panel including the options for the viewing orientation, the angle between the horizontal axis and baseline, respectively the angle between the horizontal axis and the second baseline. On the same panel are the options for size reduction and for inverting the 3D image.

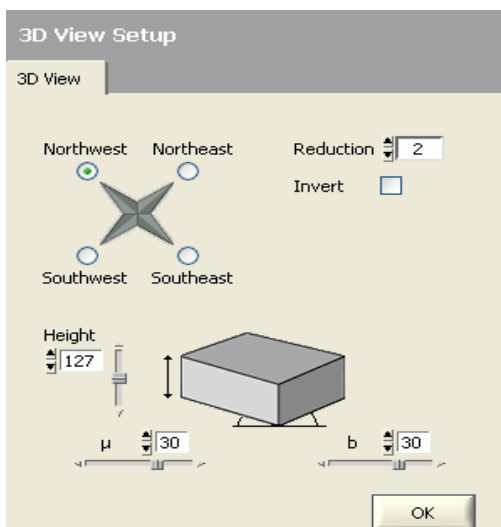


Fig.2. Settings for the 3D- echocardiography.

In Fig.3 are represented four images specific for the four view representations.

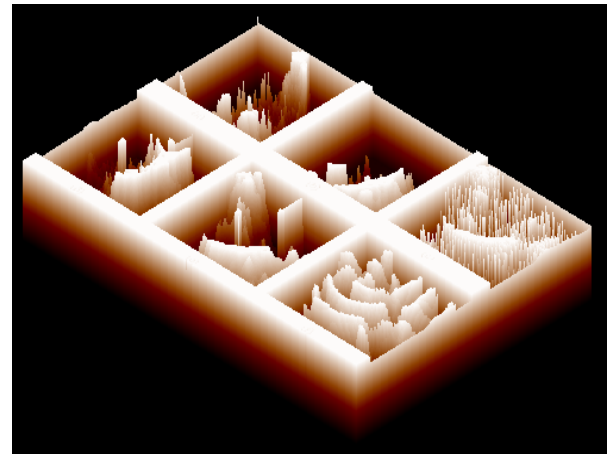


Fig.3.a. Northwest echocardiography viewing representation.

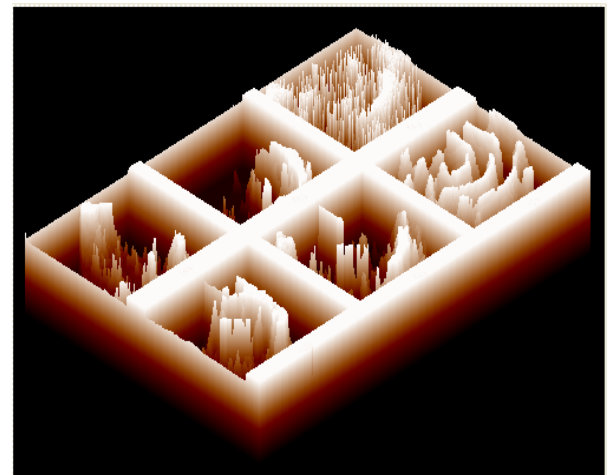


Fig.3.b. Northeast echocardiography viewing representation.

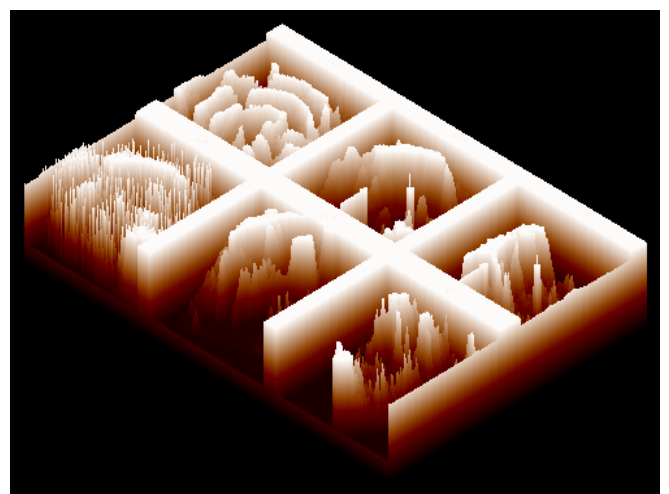


Fig.3.c. Southeast echocardiography viewing representation.

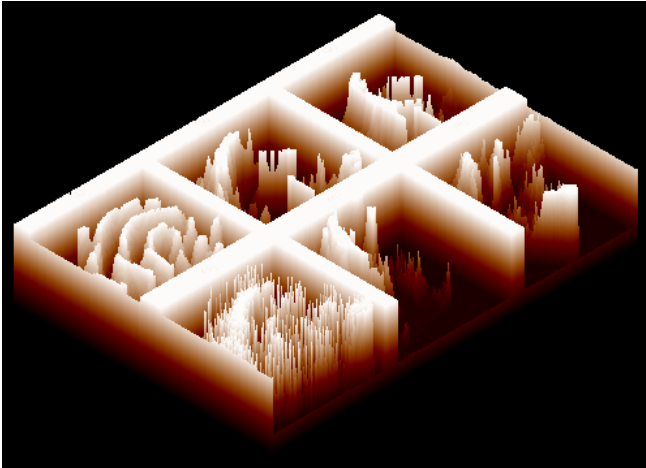


Fig.3.d. Southwest echocardiography viewing representation.

Using the LabVIEW Vision it is possible to create:

1. **Histogram:** Counts the total number of pixels in each grayscale value and graphs it.
2. **Line Profile:** Displays the grayscale distribution along a line of pixels in an image.
3. **Measure:** Calculates measurement statistics associated with a region of interest in the image.
4. **Brightness:** Alters the brightness, contrast and gamma of an image.
5. **Edge Detector:** Detects edges in grayscale images.
 - a) Straight edge (Rake): locates a straight edge in a region of interest.
 - b) Circular edge (Spoke): locates a circular edge in a region of interest.

In general, in single-modality applications, it is assumed that corresponding voxels in the two datasets from figure 1d and 1e are related by some function (the simplest case being the identity function, linked to the mean square difference similarity function), while in the multi-modality case, the most widely used voxel similarity function, mutual information [4], needs no assumption about the type of function that relates voxel intensities in the two images. In Fig.4 is represented the histogram for the selected region in a long axis registration.

Phase-based algorithms have been used in LabVIEW for a variety of tasks in image analysis, including edge detection, motion estimation, and registration. In [11], phase was calculated using a combination of steered filters, and used for image registration. A number of rules were applied to determine a weight for each image location. In [12], the authors proposed to use mutual information of

phases as the voxel metric. Results on cardiac magnetic resonance/ultrasound (MR/US) registration using a similar method were reported in [11].

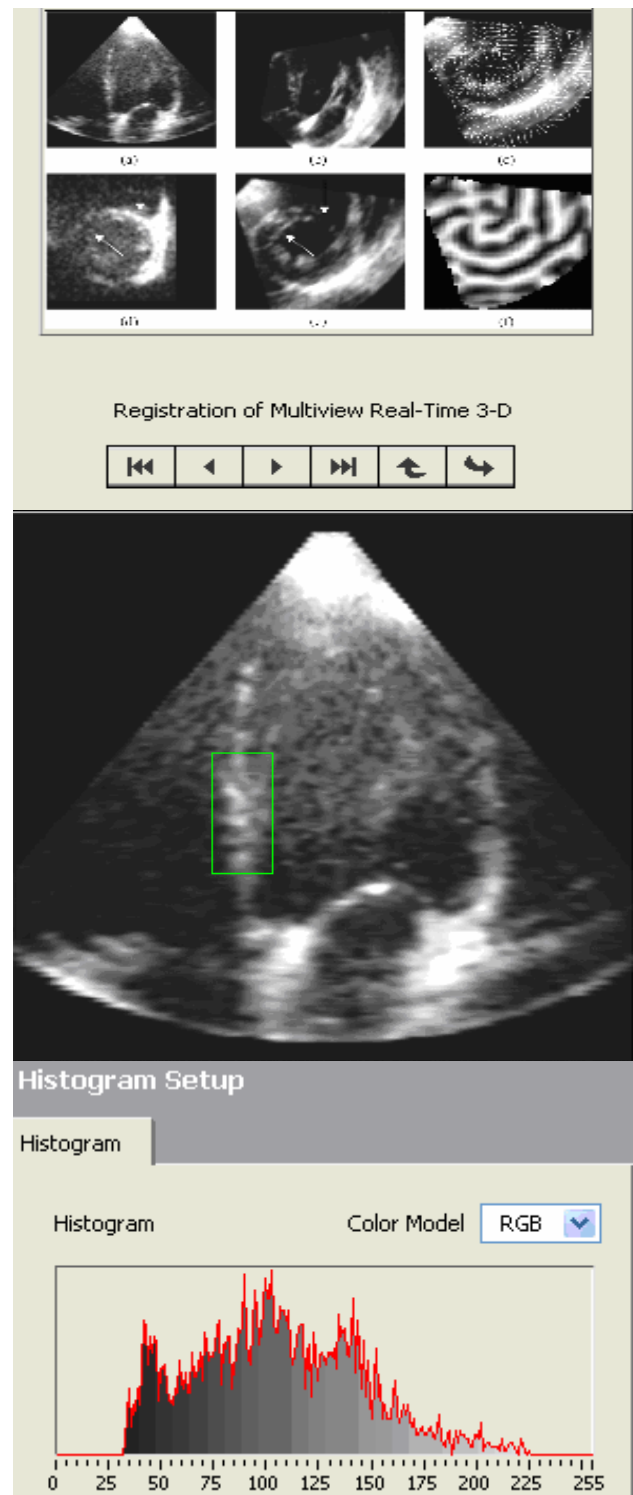


Fig.4. Histogram for the region of interest in Fig.a.

Ultrasound images have been used, due to the quality of the images and the prevalence of 2-D image acquisitions. A few authors have presented

multimodal image registration techniques involving ultrasound as one of the modalities, combining it with positron emission tomography (PET) [2], [6] or magnetic resonance imaging (MRI) [7].

Registration of cardiac images is a more complex problem than brain image registration because the heart is a nonrigid moving organ inside a moving body. Moreover, as compared to the registration of brain images, the heart exhibits much fewer accurate anatomical landmarks. In a clinical context, physicians often mentally integrate image information from different modalities. Automatic registration, based on computer programs, might, however, offer better accuracy and repeatability and save time.

In clinical practice, physicians mentally integrate information from different images acquired from a patient, often with different imaging modalities. Images are shown in various orientations and positions and at different scales. Semi-interactive registration methods rely on the expert's ability to interactively select corresponding slices using anatomical knowledge. In cardiac image registration, the semi-interactive methods are often used to register gated short axis images. In cardiac image registration, the main interest is the registration accuracy in the heart area (target registration error).

In Fig.5. is presented the script that includes the virtual instruments that execute the mentioned operations. Beginning with the original image it is possible to obtain the histogram, the line profile, statistical measurements and brightness concerning the region of interest.

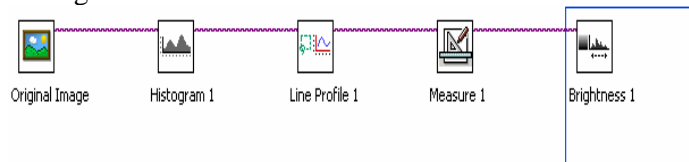


Fig.5. Script for echocardiography processing.

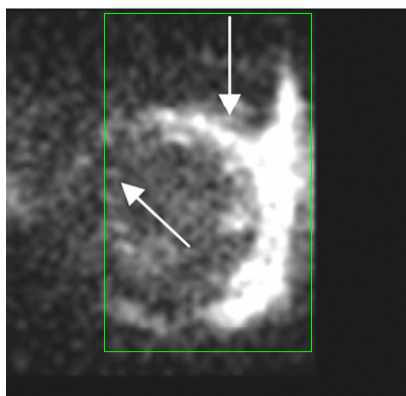


Fig.6.a. Region of interest affected by an anomaly.

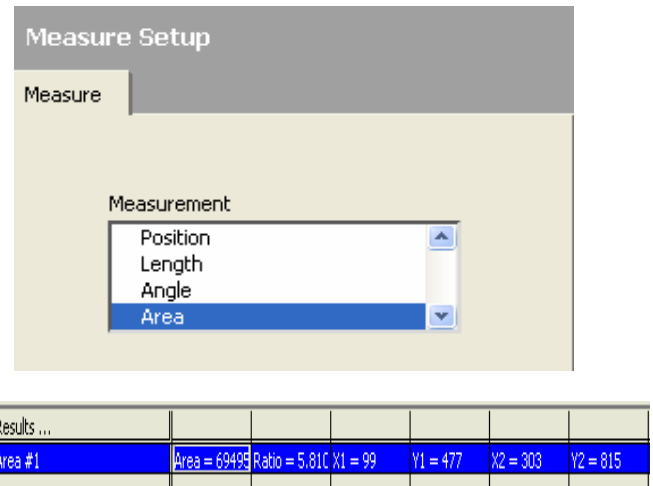


Fig.6.b. Measurement settings and results.

The LabVIEW implemented measurement setup makes it possible to determine the position, length, angle and area concerning the studied region of interest.

3. Echocardiography edge detection and filtering

One of the original contributions of this paper is to show that it is possible to get good-quality volume estimates from good-to-medium-quality 3-D echocardiography data using edge detection and filtering as processing stages.

Two-dimensional echocardiographic image edge detection and filtering are known to be challenging, and most methods only work on good-quality 2-D data [2], [5] (i.e., patients are carefully selected to have a good acoustic window and some time is taken in choosing the *best* probe position). With 3-D rotational probe imaging, there is not the luxury of optimizing each view, so edge detection and filtering methods [17], [18], [19] need to be robust to acquisition variations. The endocardial border detection literature is quite large, ranging from methods that work on the radio-frequency signal to methods that are borrowed from the computer vision literature [8], [9] to statistical methods designed for region edge detection and smoothing in noisy images [10]. We have used the feature asymmetry (FA) phase-based method of Mulet-Parada and Noble [7], [8], [11], [12]. This method which is theoretically intensity-invariant, is well suited for echocardiographic image analysis for which the intensity and contrast around the left atrium cavity varies. This approach provides accurate localization of endocardial borders in situations of changing image contrast and poor signal-to-noise ratio, and

the 2-D T version of the method provides local estimates of wall motion. However, it is well known that any phase-based method produces a large number of *spurious* noisy points. In [12], [13], [14] a dynamic programming method was proposed to link features as a postfeature detection step. We use a different grouping strategy that is more appropriate for medium-quality data. The AF algorithm is first used to produce initial feature points. We then combine spatio-temporal information relating to image acquisition with geometric constraints of the expected object shape to group endocardial edge cues.

Atrial fibrillation (AF), the most commonly encountered arrhythmia in clinical practice, is defined by the absence of coordinated atrial systole. AF results from multiple reentrant electrical wavelets that move randomly around the atria. P waves are replaced by irregular, chaotic fibrillatory waves, often with a concomitant irregular ventricular tachycardia. The rate at which the atrial electrical impulses are transmitted to the ventricle is determined by a number of factors including relative refractory period within the atrioventricular (AV) node, hydration status, and presence or absence of pharmacologic agents used to control the rate. When ventricular rate increases to tachycardic levels, a situation of atrial fibrillation with rapid ventricular response (AF with RVR) ensues. This in turn can lead to decompensation in the form of either myocardial ischemia or creation of congestive heart failure (CHF).

In the following we present an image processing chain. First the acquisition of the original image is done, afterwards the edge detector is initialized and then a straight edge and circular edge detection is applied.

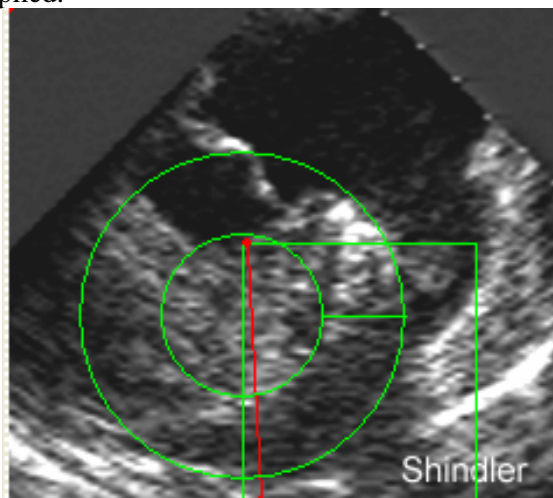


Fig.7. Transesophageal echo showing a thrombus in the left atrial appendage of a patient with atrial fibrillation.

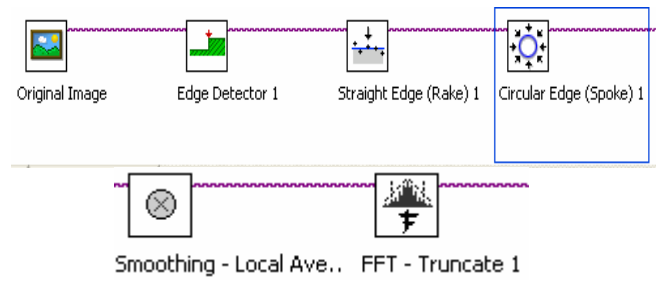


Fig.8. Atrial fibrillation straight edge, circular edge detection, smoothing and FFT truncating.

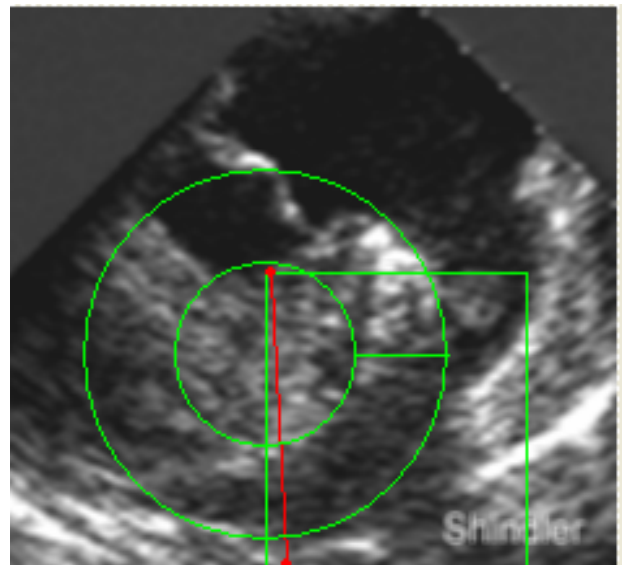


Fig.9. Atrial fibrillation image with smoothing average.

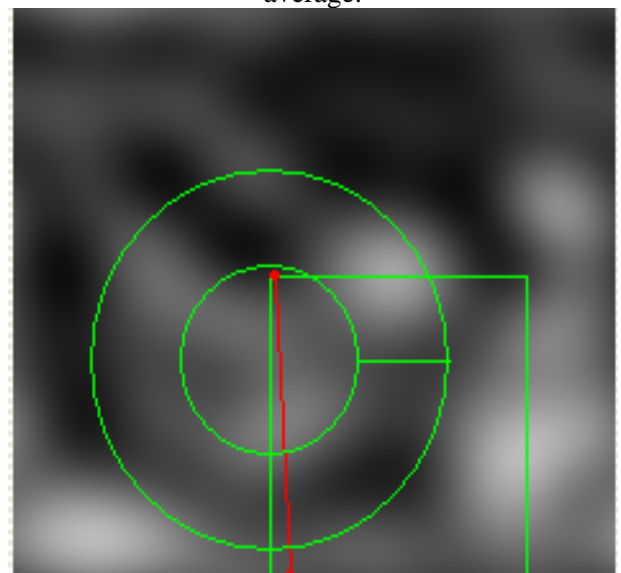


Fig.10. FFT-truncated atrial fibrillation image.

Pertinent physical findings are limited to the cardiovascular system or, if embolization has occurred, to the brain and/or peripheral vasculature.

These include the following: irregular pulse, with or without tachycardia, is typically described as the irregularly irregular rhythm. Hypotension and poor perfusion caused by decrease in atrial filling pressures and decrease in stroke volume are common findings. This may be either rate related or because of the lack of normal atrial kick. Congestive heart failure, if present, may be indicated by jugular venous distension, peripheral edema, and a gallop, which may be difficult to auscultate due to rapid rate. Signs of embolization, including transient ischemic attack (TIA), stroke, and peripheral arterial embolization (cold, pulseless extremities), may be identified. Analyzing the above images it is possible to observe the red point indicating the malfunction of the left atrium because of a thrombus in the left atrial appendage of a patient with atrial fibrillation.

4. Image acquisition and processing methods

Two-dimensional echocardiography has been a known technology for 30–40 years. Two dimensional imaging provided a significant improvement in the ability to obtain data, making it possible to scan and view planes of the heart in such a way that clinicians could visualize the anatomy of the heart [15], [16]. Using 2-D, clinicians could see both the axial and lateral dimensions, and real-time 2-D provided information about the 2-D orientation of the heart's anatomy. However, 2-D also had limitations. Since clinicians were viewing slices of the heart, they were unable to see through these walls and were not able to view the entire heart. Therefore, relying on 2-D became somewhat subjective and depended on the imagination of the person acquiring the images as clinicians were left to deduce what the complete heart image looked like. The difference between 2-D and 3-D is similar to the difference between plain X-ray and computed tomography.

Three-dimensional echocardiography moved a step closer to reality with the adoption of the transoesophageal echo (TEE) probe [20], which enabled clinicians to gain a new perspective in cardiac imaging by scanning the heart from the esophageal location, which is immediately next to or behind the heart. The OmniPlane TEE probe [20] also brought the ability to acquire multiple images of the heart from different planes for reconstruction and rendering of a triggered 3-D image. While this offered an opportunity to view the heart in 3-D using ultrasound, it also had limitations, including lack of real-time interaction of the 3-D image.

Imaging modes with the biggest impact in echocardiography all have one thing in common: real-time imaging. Every mode interacting with the image in real-time allowed for immediate decision-making.

Triggered 3-D imaging required an acquisition protocol that took many beats and required many minutes to acquire the images. The acquired data set was transferred to an offline software workstation that reconstructed and rendered the image, which added time to view the 3-D image loop. The loop was reconstructed from many beats, adding two other limiting factors: spatial discordance due to movement of the heart, transducer or patient during the acquisition process; and temporal discordance due to multiple beats of the rendered image. The process of transferring images to the offline software program was time-consuming – taking a minimum of five minutes to acquire the images and 10–15 minutes for rendering. In addition to technical issues, sedation of the patient was necessary for this unpleasant procedure (TEE), which increased potential risks to the welfare of the patient.

For image acquisition RT3DE [2] datasets were acquired from nine subjects using a Philips Sonos 7500 scanner at the John Radcliffe Hospital, Oxford, U.K. Between 1 and 5 parasternal datasets and between 1 and 6 apical ones were obtained for each subject. When more than one acquisition from the same window was done, the angle of the probe was deliberately changed between acquisitions, to vary the information contained on each dataset.

The new real-time 3D acquisition system is designed for superb clinical performance, improved productivity and advanced research. This real-time 3D acquisition system becomes even more powerful with the addition of the Performance 2005 upgrade. Designed for maximal flexibility, the presented system can be purchased with the advanced features we need today and remain ready for additional capabilities as our needs change. These new and revolutionary enhancements allow workflow efficiencies that simply aren't possible with conventional echo systems. For example, we can now network real-time 3D images and data sets, review and quantify real-time 3D data off-line, and improve the productivity of a stress echo exam with this system and LabVIEW. In figure 11 we shall see an image of the ovine mitral valve leaflet created using data obtained from real-time 3-D echocardiography.

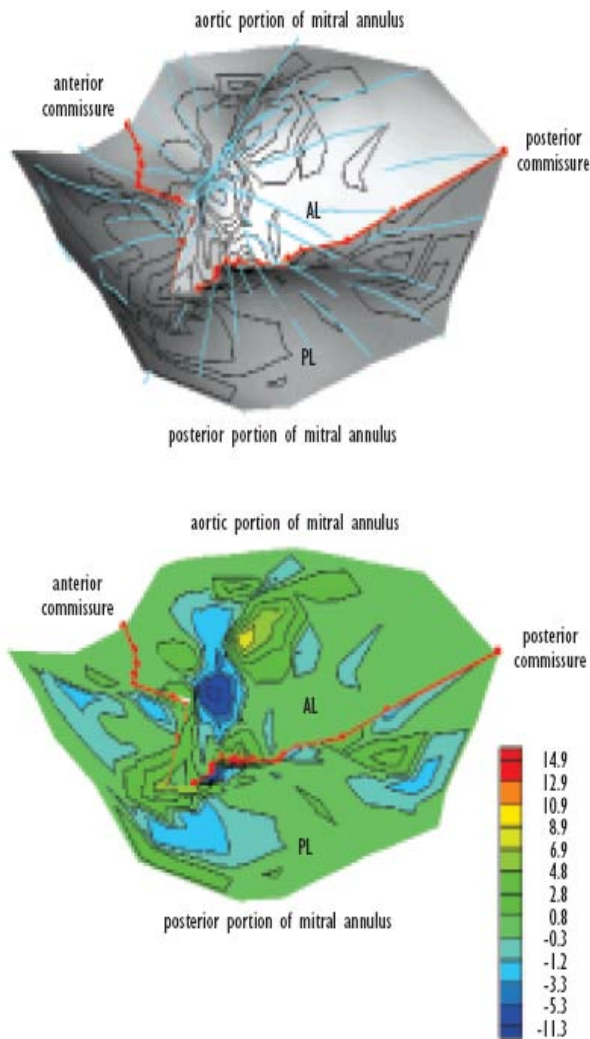


Fig. 11. Echocardiography using a 3-D real-time acquisition.

Four clinical situations where *real-time 3D echocardiography acquisition* can impact directly on the quality of patient care are presented in [9]. The first is the diagnosis of congenital heart disease. Many of these disorders are caused by complex geometrical distortions of cardiac anatomy. Currently, a combination of 2-D echocardiography and cardiac catheterization is used to diagnose these diseases. Real-Time 3-D echocardiography will provide more detailed information with one noninvasive test.

Another surgical application is in the planning and assessment of mitral valve repair. Current 2-D echo provides good information regarding valve deformations, but it is not uncommon for the surgeon to find different or additional abnormalities in surgery than were identified pre-operatively by current echo techniques. Since these observations of surgery are made in an arrested and flaccid heart, it is sometimes difficult for the surgeon to determine their importance to valve competence. Real-time

3-D echo acquisition will allow a more complete *dynamic* assessment of valve dysfunction.

A reasonably good starting point is required to avoid the optimization method from getting trapped in a local minimum. In the case of multi-window acquisition, the misalignment between the original datasets is too large for registration algorithms to converge to the global minimum. Though it is possible to calculate an approximate probe location valid for most or all subjects, based on an estimation of approximate apical and parasternal positions for the general case, but it will be still the problem to estimate the approximate rotation of the probe about its axis, which in the 3-D acquisitions can be modified by the clinician. A landmark-based initialization has been chosen. Three landmarks are identified, corresponding to the hinges of the mitral and aortic valves. Selection of the landmarks was done on the end-diastolic frame, by manually locating a slice crossing approximately through the centers of the mitral and aortic valve rings and parallel to the long axis of the left ventricle. On this image, the hinge points were manually identified. In Fig. 2, these planes with the landmarks detected in a sample case are shown. Note that the center landmark corresponds to the hinges of both the mitral and aortic valves, and is located between them. The rigid transform that minimizes the sum of squared distances between landmarks is chosen as initialization.

$$T_{ini} = \arg \min \sum_{i=1}^3 \| l_i^{api} - T(l_i^{par}) \|^2 \quad (2)$$

where l_i^{api} and l_i^{par} are the coordinates of the apical and parasternal i th landmark, respectively, and is the result of applying transform to point . Calculation of the minimum in (2) was done using the singular value decomposition method as described in [2], [20]. Applying LabVIEW and Vision the valve hinges have been highlighted in Fig.12.

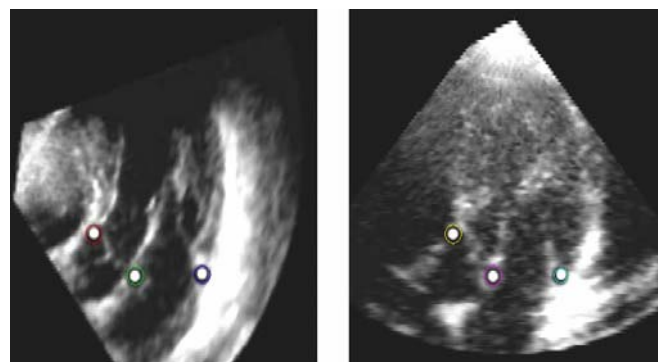


Fig.12. Slices of the parasternal (left) and apical (right) datasets of a sample subject with the points corresponding to the valve hinges highlighted.

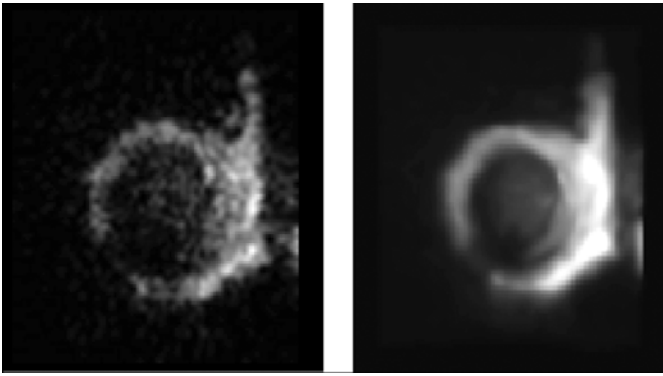


Fig.13. Original (left) and filtered (right) sample images from an apical RT3DE dataset.

In LabVIEW and Vision was implemented an edge algorithm and a despeckling filter and we obtained fig.14.a and fig.14.b.

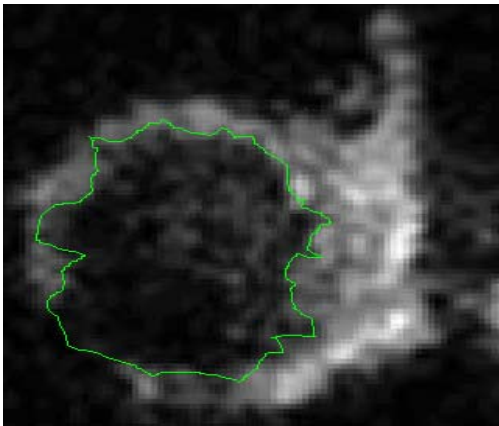


Fig.14.a.Edge contour for an apical RT3DE image.

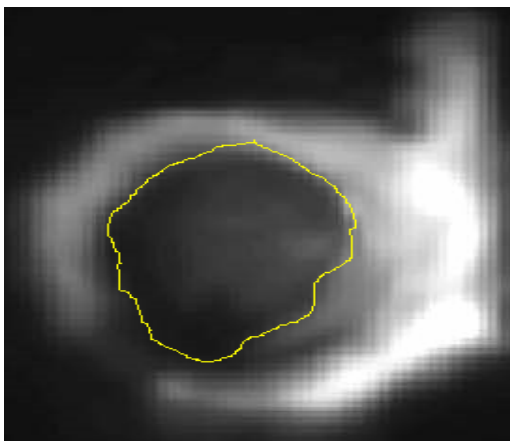


Fig.14.b.Edge contour for an apical RT3DE image after applying a despeckling filter.

In Fig.15.a. and Fig.15.b are represented two different positions for echocardiography for better seeing the anterior mitral leaflet and ruptured chords.

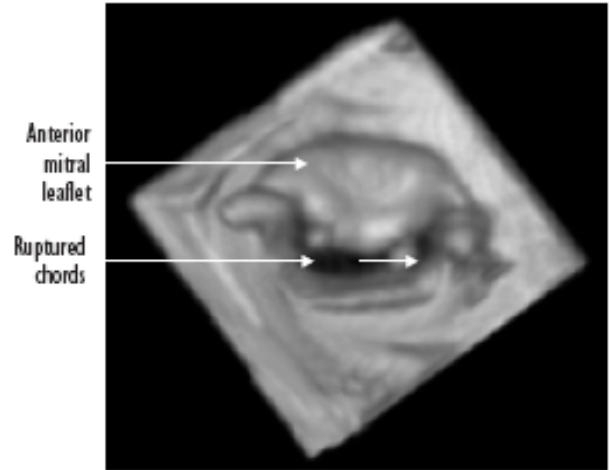


Fig.15.a. RT3D echocardiography left side acquisition.

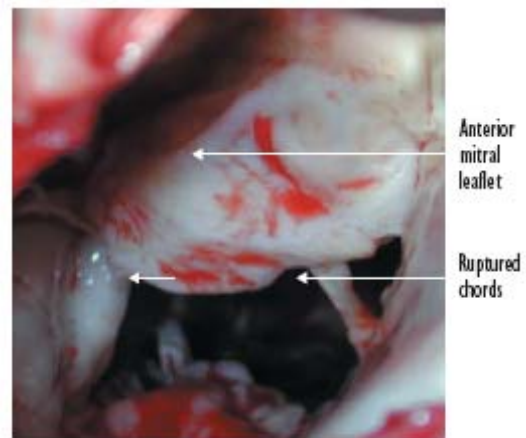


Fig.15.b. RT3D echocardiography right side acquisition.

The next step applies in LabVIEW and Vision a threshold to the three planes of a color image and places the results into an 8bit image.



Fig.16.a. Threshold applied to a RT3D echocardiography color image.

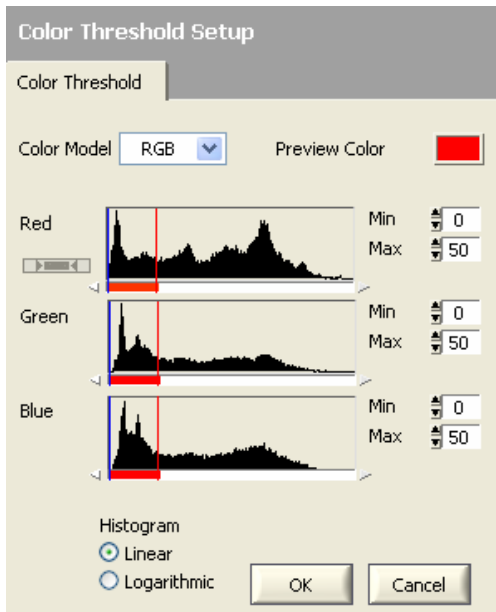


Fig.16.b. Color threshold applied to a RT3D echocardiography.



Fig.17. Symmetry.

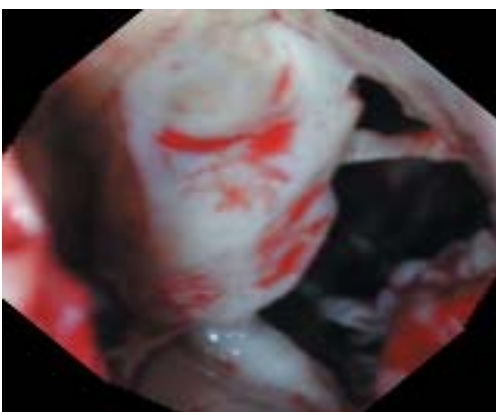


Fig.18. Rotation 135 degrees.

Even in low-contrast areas of the image, the symmetry and rotation algorithm returns a reasonable value for orientation. Notice that, at the central line of ridges, artefacts in orientation may

appear. These are locations where the phase is close to zero, and thus have a low orientation confidence.

Speckle present in echocardiographic images can convey important information to the clinicians about heart function, and has been used in edge detection, filtering and motion detection [2], [20], [21], [22], [23]. When registering images acquired from the same window (e.g., two consecutive frames from the same sequence), matching speckle patterns contributes to calculate the correct geometric transform. However, our case differs significantly from previous ones in that, due to the large difference in probe position, speckle patterns are in general uncorrelated and thus can be a source of artifacts. For this reason, we apply an initial filtering step that removes speckle while keeping the main anatomical structures in the images. Several despeckling filters have been proposed: see e.g., [15]–[17]. Most of them require access to the envelope image (before logarithmic correction) or an estimation of parameters that describe the logarithmic correction step [17]. Envelope detected images are not available in our case, and are in general not provided by the manufacturers of U.S. equipment. In this case, we use coherence-enhancing edge detection, first proposed by [18] and which has been demonstrated to reduce the speckle content of echocardiographic images. In Fig. 3, an example of RT3DE dataset filtered in this way is shown. As can be appreciated in the images, all major structures, which will be necessary to calculate the voxel similarity measure, are maintained in the filtered images, while speckle and general noise, which would affect the performance of the algorithm, are removed. Further details about the use of the filter can be found in [19]. In 1-D signals, local phase can be derived from the analytic signal, constructed using the original signal and its Hilbert transform. There is no unique way to extend the concept to the N-dimensional case. A commonly used possibility is to use a bank of steerable filters [17], [18], [19]. In [19] and [20], the monogenic signal, an isotropic extension of the analytic signal to an -dimensional space, was proposed. In this section, a simplified explanation of the monogenic signal is given. The reader is referred to [2], [19] and [20] for details. The monogenic signal is based on the Riesz transform, an-dimensional generalization of the Hilbert transform. The Riesz transform is calculated by applying a set of filters (being the number of dimensions) to the image. In the 3-D space, the filters are given, in the Fourier domain, by

$$\begin{aligned}
 H_1(u, v, w) &= \frac{u}{\sqrt{u^2 + v^2 + w^2}} \\
 H_2(u, v, w) &= \frac{v}{\sqrt{u^2 + v^2 + w^2}} \\
 H_3(u, v, w) &= \frac{w}{\sqrt{u^2 + v^2 + w^2}}
 \end{aligned} \quad (3)$$

where u , v , w are the Fourier domain coordinates. To achieve frequency localization as well as spatial localization, a bandpass filter is applied to the signal prior to calculating the monogenic signal. In our case, we used log-Gabor filters. The monogenic signal assigns an - dimensional vector (the combination of the original signal value and the Riesz transform) to each spatial location. The angles that define the vector can be used to estimate the D local signal orientation and phase. Specifically, in the 3-D case orientation and phase can be calculated as in [16], [17], and [18]. The normalized orientation vectors calculated at scale represents the bandpass filter with a central wavelength and is the spatial versions of the filters described in [17], [18], and [19].

5 Conclusion

One such advancement is the presented *real-time 3D image acquisition*. While three-dimensional (3-D) technology in cardiac ultrasound is not a new concept – it has been well known as a clinical application for the last 12–13 years – the use of *real-time 3D biomedical images acquisition* as a clinically viable application is new. Historically, 3-D echocardiography involved the compilation of multiple 2-D images. However, the overall image acquired was not in real-time. That has all changed within the past 18 months as technology has evolved to make real-time imaging in 3-D possible. As a result, we are now able to diagnose potentially life-threatening medical conditions in real-time, and doctors are better able to communicate the diagnosis and make recommendations for treatment without any guesswork. The importance of real-time 3-D cannot be emphasized enough. It gives us different levels of knowledge – such as viewing and diagnosing problems with the mitral valve – that could not be obtained before. It is the real-time aspect of this technology that is critical in obtaining a precise diagnosis.

Various echocardiographic techniques have been used to assess dyssynchrony in those with heart failure, in the presence or absence of a wide QRS complex. All studies to date, however, have either been retrospective or small prospective studies.

An algorithm for three dimensional representations has been implemented using scripts written in LabVIEW for National Instruments Vision considering the RT3DE datasets. The algorithm is based on structure orientation and phase. This reduces sensitivity to image brightness and contrast, a desirable feature when processing ultrasound images. Initialization is done by selecting three landmarks in each of the datasets, corresponding to points on the mitral and aortic valve rings.

Qualitative and quantitative validation shows excellent accuracy and sufficient robustness against changes in the initialization landmarks. Datasets combined using the presented algorithm have the potential of improving accuracy and robustness of quantitative 3-D cardiac functional analysis.

The implemented LabVIEW scripts for Vision solve a lot of problems concerning the 3D-image processing.

Having addressed and resolved the technological and practical issues, Real-Time 3D imaging has great potential to impact both patient care and improve pre and post-surgical planning. In 3D real-time images of the heart are displayed instantly on the monitor as a patient is scanned, without stopping to render images. As a result, we are able to provide immediate and improved perspective on the heart's size and shape and interrelationships between valves, chambers and vessels.

Providing a 3-D image of the heart gives physicians a complete view from multiple perspectives – images that were not available using conventional 2-D echocardiography. Using 3-D, images can be rotated and cropped to view the heart from all angles, which enables the physician to make a more accurate diagnosis. In other words, 3-D is similar to holding the heart in your hands, compared with 2-D, which left physicians having to visualize the heart.

The degree of precision is completely different from a previously used baseline cardiac examination. The degree of knowledge gained as a result can be put into action, moving medical science forward. This in-depth knowledge is, without doubt, a major advantage to surgeons.

References:

- [1] I. Herlin and N. Ayache, Feature extraction and analysis methods for sequences of ultrasound images, in *Proc. Eur. Conf. Computer Vision*, 1992, pp. 43–57.
- [2] V. Grau, H. Becher, and J. A. Noble Registration of Multiview Real-Time 3-D

- Echocardiographic Sequences, *IEEE Transactions on medical imaging*, vol. 26, no. 9, September 2007, pp. 1154-1165.
- [3] G. Coppini, R. Poli, and G. Valli, Recovery of the 3D shape of the left ventricle from echocardiographic images, *IEEE Trans. Med. Imag.*, vol. 15, no. 6, pp. 301–317, 1995.
- [4] Xujiang Ye, J. Alison Noble, David Atkinson, 3-D Freehand Echocardiography for Automatic Left Ventricle Reconstruction and Analysis Based on Multiple Acoustic Windows, *IEEE Transactions on Medical Imaging*, vol. 21, no. 9, September 2002.
- [5] D. Boukerroui, J. A. Noble, and M. Brady, Feature enhancement in low quality images with application to echocardiography, *Ultrasound Med. Biol.*, vol. 27, no. 12, pp. 1583–1594, 2001.
- [6] M. Handke and D. M. Schäfer *et al.*, Improved 3D echocardiographic endocardial border delineation using the contrast agent FS069 transesophageal studies in a porcine model, *Ultrasound Med. Biol.*, vol. 27, no. 9, pp. 1185–1190, 2001.
- [7] M. Mulet-Parada, Intensity Independent Feature Extraction and Tracking in Echocardiographic Sequences, Ph.D., University of Oxford, 2000.
- [8] M. Mulet-Parada and J. A. Noble, “2D + T boundary detection in echocardiography,” in *Proc. MICCAI*, Cambridge, MA, 1998, pp. 186–196.
- [9] J. Gorman, The role of live 3D echocardiography key in cardiac research efforts, *Global Surgery 2003*, extract.
- [10] Y. Katsnelson, Live 3D Echo Facilitates Faster, More Accurate Cardiac Diagnoses Improving Patient Care, *Global Surgery 2003*, extract.
- [11] W. Zhang, J. A. Noble, and M. Brady, Real time 3-D ultrasound to MR cardiovascular image registration using a phase-based approach, in *IEEE Int. Symp. Biomed. Imag.: From Nano to Macro*, pp. 666–669, Apr. 2006.
- [12] M. Mellor and M. Brady, Phase mutual information as a similarity measure for registration, *Med. Image Anal.*, vol. 9, pp. 330–343, 2005.
- [13] K. S. Arun, T. S. Huang, and S. D. Blostein, Least square fitting of two 3-d point sets, *IEEE Trans. Pattern Anal. Mach. Intell.*, vol. 9, pp. 698–700, Sep. 1987.
- [14] J. A. Noble and D. Boukerroui, Ultrasound image segmentation: A survey, *IEEE Trans. Med. Imag.*, vol. 25, no. 8, pp. 987–1010, Aug. 2006.
- [15] A. Achim, A. Bezerianos, and P. Tsakalides, Novel Bayesian multiscale method for speckle removal in medical ultrasound images, *IEEE Trans. Med. Imag.*, vol. 20, no. 8, pp. 772–783, Aug. 2001.
- [16] X. H. Hao, S. K. Gao, and X. R. Gao, A novel multiscale nonlinear thresholding method for ultrasonic speckle suppressing, *IEEE Trans. Med. Imag.*, vol. 18, no. 9, pp. 787–794, Sep. 1999.
- [17] V. Dutt and J. F. Greenleaf, Adaptive speckle reduction filter for logcompressed B-scan images, *IEEE Trans. Med. Imag.*, vol. 15, no. 6, pp. 802–813, Dec. 1996.
- [18] J. Weickert, Coherence-enhancing diffusion filtering, *Int. J. Computer Vision*, vol. 31, pp. 111–127, 1999.
- [19] V. Grau and J. A. Noble, Motion-guided anisotropic filtering of ultrasound sequences, in *IEEE International Symposium on Biomedical Imaging: From Nano to Macro*, Apr. 2006, pp. 209–212.
- [20] R. Vorray, V. Grau, J. Noble, and H. Becher, HeartBeat, A tool to compare and align 3-D cardiac data sets of different imaging modalities, presented at the *EuroEcho9*, Florence, Italy, 2005.
- [21] Th. Panagopoulos, C. Papaodysseus, M. Exarhos, C. Triantafillou, G. Roussopoulos, P. Roussopoulos, Prehistoric Wall-Paintings Reconstruction Using Image Pattern Analysis And Curve Fitting, *Wseas Transactions on Electronics*, Issue 1, Volume 1, January 2004, ISSN:1109-9445, pp.108-104.
- [22] R. Farjam, H. Soltanian-Zadeh, R. A. Zoroofi, Wavelet Based Determination of Malignancy of the Pathological Images of the Prostate, *Wseas Transactions on Electronics*, Issue 3, Volume 1, July 2004, ISSN:1109-9445, pp.476-482.
- [23] M. T. Oraiqt, F. M. Awwad, H. M. Al-Otum, A Comparison of Image Enhancement using Curvelet transform with multiscale gradient and Retinex Operators, *Wseas Transactions on Electronics*, Issue 3, Volume 1, July 2004, ISSN:1109-9445, pp.461-467.